Theoretical Analysis and Experimental Study of Time-Varying Electric Field and Electrostatic Adhesion Force Generated by Interdigital Electrode Arrays

Rui Chen* , Xiaohong Chen, Long Bai and Qian Tang

State Key Laboratory of Mechanical Transmissions, Chongqing University, Chongqing 400044, China

Abstract: A theoretical model is presented for the analysis of the electric field and electrostatic adhesion force produced by interdigital electrode arrays. The electric field is derived by solving the Laplace equation for the electrical potential in each subregion. The electrostatic adhesion force is calculated using the Maxwell stress tensor formulation. The dynamic properties of the electric field and electrostatic adhesion force are assessed by evaluating the transient response of the field and force under a step in applied voltages. Experimental studies are carried out to evaluate the adhesion performance of an electrode panel on a glass pane, and the experimental results verify the correctness of the theoretical model.

Keywords: Electrostatic adhesion force, electric field, interdigital electrode arrays, modelling, dynamic properties.

1. INTRODUCTION

Electrostatic force has found widespread uses in many application areas [1], the most well-known being laser printing, dust cleaning and cathode ray tube technology used for televisions and computer screens. In recent years, considerable interest has been placed on the development of various electrostatic devices applied in industrial areas. The electrostatic chuck used for wafer handling or workpiece fixing in semiconductor manufacture is one of the most important applications [2, 3]. Such electrostatic chuck possesses several advantages compared with a mechanical holding system. Since the electrostatic force is uniformly distributed over the object's surface, an electrostatic chuck can hold the object flat, avoiding the common problem of structure deformation in the process of mechanical manipulation. Furthermore, an electrostatic chuck can transport a wafer faster, and thus improve the production yield, while a mechanical gripper requires low speed movement to avoid particle generation. Electrostatic suspension is another effective application similar to the electrostatic chuck [4-6]. This noncontact holding system can not only avoid structure deformation of the material, but also circumvent surface contamination and particle generation. Dielectrophoresis is one of the AC electrokinetic techniques, which is now used for analysis and separation of biological particles, such as cells, bacteria and viruses [7-10]. Polarizable particles move towards or away from regions of strong field by dielectrophoresis force. The force levitates different particles to different heights producing a vertical separation. Electrostatic adhesion, as an electrically controllable adhesion technology, is applied to wall-climbing robots for the first time [11-13]. It involves inducing electrostatic charges on a wall surface by using a power supply connected to compliant pads placed on the moving robot. Using this technology, various wall-climbing robots have been demonstrated, including robots with feet and tracks.

In all the applications above, electrostatic force generated on the object is obtained by exerting the voltages to the shaped electrodes. Among many different types of electrodes examined, interdigital electrodes show the best features [2]. The interdigital electrode arrays are similar, consisting of a large number of thin parallel bar electrodes fabricated on a flat substrate. As we know, the electrostatic force is directly dependent on the electric field. Thus knowledge of the electric field and the electrostatic force generated by the interdigital electrodes is essential for improving the work performance of these applications.

However, due to the nonuniformity of the electric field generated by the interdigital electrode arrays, modelling and analysis of the electric field (and as a result the electrostatic adhesion force) is not an easy work. So far, the electric field for an interdigital electrode array has been solved mainly by numerical methods, such as point charge [14], charge density [15], finite element [7], finite difference and integral equation methods [16], as well as analytical approximation based on Green's functions [8], point matching [17], conformal mapping [9] and Fourier

*Address correspondence to this author at the State Key Laboratory of Mechanical Transmissions, Chongqing University, Chongqing 400044, China; Tel: (+86) 15736270849; Fax: 023-65105795; E-mail: cr@cqu.edu.cn

© 2014 Avanti Publishers

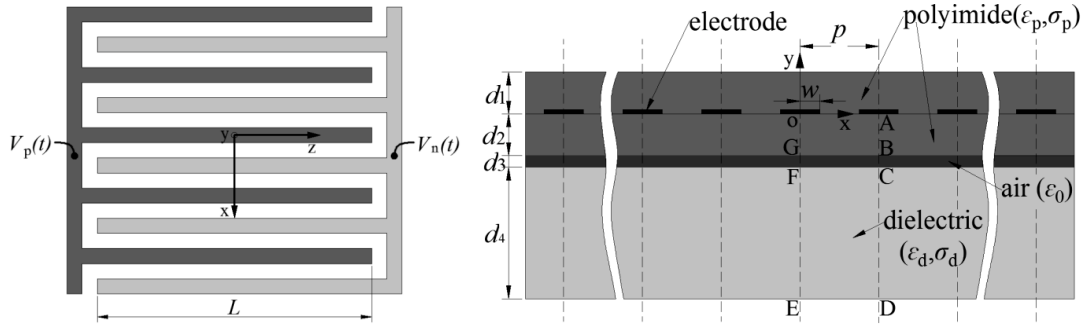

(**a**) (**b**)

Figure 1: (**a**) Layout of interdigital electrode arrays. (**b**) Cross-section of the adhesion model.

series [10]. All of the numerical methods suffer from the problem of intensive computation and low accuracy, and can-not provide enough theoretical guidance for the actual application, such as the optimization of the proposed electrode configurations. An analytical approach to field determinations is desirable to provide more rapid and accurate solutions. However, some of the existing methods mainly aim at some specific application areas, such as dielectrophoresis and electrostatic suspension [18], where the electrode arrays are usually placed in a single homogeneous medium. In addition, there are few literatures concerning the dynamic properties of the electric field and the electrostatic adhesion force.

The aim of this paper is to develop an analytical model for the electric field and electrostatic adhesion force generated by the interdigital electrode arrays. A typical adhesion system consisting of an electrode panel and a dielectric plate positioned below the electrode panel is considered. The electric field problem involves solving the Laplace equations with the boundary conditions taken into account. Based on this model, field and force dynamics are investigated as a function of structure parameters of the electrode panel and electrical parameters of the system. Experiments are carried out to evaluate the adhesion performance of the electrode panel on the glass pane, and the experimental results verify the correctness of the theoretical model. Finally, we discuss an approximation of the inter-electrode potential and truncation of series expansion of the field components. The influence of vacuum suction force on the adhesion system is also discussed.

2. THEORETICAL DERIVATION

2.1. Physical Model

A basic model that can adequately describe the performance of the interdigital electrode arrays is depicted in Figure **1**. In this model, the electrode structure consists of two interpenetrating comb electrodes, each having a number of fingers of length *L*. Time-varying electric potentials $V_p(t)$ and $V_n(t)$ are exerted on the electrodes. The electrodes are of width 2*w* and are spaced equidistantly with pitch *p*. The electrodes, made of copper in general, are deposited on a polyimide film with a thickness of d_2. Another polyimide film of thickness d_1 is covered on the electrodes for electric insulation. Both of the two polyimide films have uniform permittivity ε_p and volume conductivity σ_p. The polyimide films and the copper electrodes sandwiched between the two films constitute an electrode panel, which is used to generate electric field and force under a voltage excitation. Positioned below the electrode panel is a dielectric plate with the thickness being d_4, uniform permittivity being ε_d and volume conductivity being σ_d. Given the roughness of the dielectric surface, a simplified thin air layer with a thickness of d_3 is taken into account between the electrode panel and the dielectric plate.

2.2 Basic equations and assumptions

Since currents are varying at a sufficiently small rate, Maxwell's equations can be reduced to the quasi-electrostatic form [19]:

$$\mathbf{E} = -\nabla\phi \tag{1}$$

$$\nabla \cdot \mathbf{D} = \rho \tag{2}$$

$$\nabla \cdot \mathbf{J} + \frac{\partial \rho}{\partial t} = 0 \tag{3}$$

where $\mathbf{E}$ is the electric field, $\mathbf{D}$ is the electric flux density or the displacement vector, ρ is the free charge density, and $\mathbf{J}$ is the conduction current. For a homogeneous linear dielectric with permittivity ε and conductivity σ, $\mathbf{D} = \varepsilon\mathbf{E}$ and $\mathbf{J} = \sigma\mathbf{E}$.

Given the particular interdigital electrodes, some simplifications and assumptions can be made. Since electric field is generated mainly between neighbouring comb fingers, we simplify the comb electrodes into a planar array of parallel strip electrodes without consideration of the effect of the root segments of the electrodes. As the length of electrodes (*L*) is much larger than the width of them (2*w*) and the thickness of air layer (d_3), the edge effect along the length direction can be ignored. In addition, the electric field along the length direction is uniform, so we can transform this 3D problem into a 2D one by taking the cross-section of the electrode panel into consideration. Due to the periodicity of the electrode structure, we can choose one period as the research object, which is the region of $0 \le x \le p$. From Figure **1**, it is evident that the electrode structure is even symmetry along the centerlines, so the problem space required for the correct solution to the electric field problem can be reduced to the region bounded by OADE.

Due to the presence of the stratified dielectric mediums, the electric field exhibits discontinuities on boundaries GB and FC. For this reason, the problem space is divided into three rectangular piece-wise uniform subregions: OABG, GBCF and FCDE. In the following, we shall denote these regions as subregions 1, 2, and 3. In each subregion, the potential is a solution of Laplace equation, which in an isotropic medium, assumes the form:

$$\frac{\partial^2 \phi(x,y,t)}{\partial x^2} + \frac{\partial^2 \phi(x,y,t)}{\partial y^2} = 0 \tag{4}$$

where $\phi(x,y,t)$ is the spatial time-varying potential distribution. By using the method of separation of variables [19], i.e., assuming $\phi(x,y,t) = X(x,t)Y(y,t)$, the partial differential equation (4) can be transformed into two ordinary differential equations:

$$\frac{d^2 X(x,t)}{dx^2} + \lambda^2 X(x,t) = 0,$$

$$\frac{d^2 Y(y,t)}{dy^2} - \lambda^2 Y(y,t) = 0, \tag{5}$$

where λ is the separation constant. Independent particular solutions $\phi_{\lambda=0}(x,y,t)$ and $\phi_{\lambda\neq 0}(x,y,t)$ can be obtained by solving equation (5) for the two separate cases $\lambda = 0$ and $\lambda \neq 0$, respectively. A general solution to equation (4) can be derived as a combination of $\phi_{\lambda=0}(x,y,t)$ and $\phi_{\lambda\neq 0}(x,y,t)$:

$$\begin{aligned}\phi(x,y,t) = \phi_{\lambda=0}(x,y,t) + \phi_{\lambda\neq 0}(x,y,t) = [A(t)x + B(t)] \\ [C(t)y + D(t)] + [E(t)\sin(\lambda x) + F(t)\cos(\lambda x)] \times \\ [G(t)\sinh(\lambda y) + H(t)\cosh(\lambda y)].\end{aligned} \tag{6}$$

The arbitrary time-varying coefficients $A(t)$, $B(t)$, $C(t)$, $D(t)$, $E(t)$, $F(t)$, $G(t)$, $H(t)$, and the separation constant λ are determined such that $\phi(x,y,t)$ satisfies the boundary conditions.

2.3. Boundary Conditions

The three subregions which make up the problem space have in common that the potential in each subregion is finite and symmetry on the planes $x = 0$ and $x = p$, therefore, the Neumann-type boundary conditions should be followed:

$$\frac{\partial \phi(0,y,t)}{\partial x} = 0, \quad \frac{\partial \phi(p,y,t)}{\partial x} = 0, -(d_2 + d_3 + d_4) \le y \le 0. \tag{7}$$

Since the electrodes are much thinner than their width, we ignore the thickness so that the potential on the electrodes is specified at $y = 0$. The potential distribution on the positive and negative electrodes is specifically described by the applied voltages $V_{\mathrm{p}}(t)$ and $V_{\mathrm{n}}(t)$. However, this is not a complete boundary condition of the potential distribution on the entire electrode plane because the electrodes do not form a closed surface and the potentials in the inter-electrode gap are unknown. Here for clarity and convenience, we will take the first-order Taylor series approximation by assuming that the potential varies linearly with distance in the electrode gaps (an approach for determining the complete boundary potential conditions will be described later). Thus the boundary conditions for our model are given by

$$\phi(x,0,t) = \begin{cases} V_{\mathrm{p}}(t) & 0 \le x \le w \\ \dfrac{V_{\mathrm{p}}(t) + V_{\mathrm{n}}(t)}{2} + [V_{\mathrm{n}}(t) - V_{\mathrm{p}}(t)]\dfrac{x - p/2}{p - 2w} & w < x < p - w \\ V_{\mathrm{n}}(t) & p - w \le x \le p \end{cases}. \tag{8}$$

The analytical expression for the potential on the boundary plane $y = 0$ is piecewise smooth in the interval $0 \le x \le p$. By using Fourier series expansion, we can obtain an expression that is continuously smooth in the interval $0 \le x \le p$, which is convenient for subsequent discussions. As this potential is an even function with respect to the *y*-axis, only the cosine terms are retained in its Fourier series representation:

$$\phi(x,0,t) = \frac{a_0(t)}{2} + \sum_{n=1}^{\infty} a_n(t)\cos\left(\frac{n\pi x}{p}\right) \quad 0 \le x \le p \tag{9}$$

where

$$a_n(t) = \frac{2}{p}\int_0^p \phi(x,0,t)\cos\left(\frac{n\pi x}{p}\right)dx \quad (n = 0, 1, 2, \ldots). \tag{10}$$

Substitution of equation (8) and equation (10) into equation (9) yields the following Fourier series representation of the electric potential on the boundary $y = 0$:

$$\phi(x,0,t) = \frac{V_p(t)+V_n(t)}{2} + \frac{2[V_n(t)-V_p(t)]}{\pi^2(1-2w/p)} \times \sum_{n=1}^{\infty} \frac{1}{n^2}[\cos(n\pi - \frac{n\pi w}{p}) - \cos(\frac{n\pi w}{p})]\cos(\frac{n\pi x}{p}) \quad 0 \le x \le p \tag{11}$$

Boundary conditions related to the three rectangular piece-wise uniform subregions can be divided into two parts, which are with respect to the two dielectric interfaces. The boundary conditions representing the irrotational condition of the electric field can be given by

$$\begin{aligned} &\mathbf{n} \times (\mathbf{E}_1 - \mathbf{E}_2) = 0, \quad y = -d_2 \\ &\mathbf{n} \times (\mathbf{E}_2 - \mathbf{E}_3) = 0, \quad y = -(d_2 + d_3). \end{aligned} \tag{12}$$

The boundary conditions associated with the charge conservation law (or the continuity of current) at the two dielectric interfaces can be written as [20]

$$\begin{aligned} &\frac{\partial}{\partial t}\mathbf{n} \cdot (\varepsilon_p \mathbf{E}_1 - \varepsilon_0 \mathbf{E}_2) + \mathbf{n} \cdot (\sigma_p \mathbf{E}_1) = 0, \ y = -d_2 \\ &\frac{\partial}{\partial t}\mathbf{n} \cdot (\varepsilon_0 \mathbf{E}_2 - \varepsilon_d \mathbf{E}_3) - \mathbf{n} \cdot (\sigma_d \mathbf{E}_3) = 0, \ y = -(d_2 + d_3) \end{aligned} \tag{13}$$

where ***n*** is the unit vector of the *y* axis , $\mathbf{E}_1$, $\mathbf{E}_2$ and $\mathbf{E}_3$ are the electric field in subregions 1, 2 and 3, respectively.

In general, since the thickness of the dielectric plate is much larger than that of the polyimide film and the air layer ($d_4 >> d_2, d_4 >> d_3$), d_4 is usually treated as infinity for reasonable simplification. The last boundary condition expresses that the potential decays to zero when *y* approaches infinity, that is:

$$\lim_{y \to -\infty} \phi(x,y,t) = 0. \tag{14}$$

Equations (7), (11), (12), (13) and (14) constitute the complete set of boundary conditions necessary to solve the posed boundary problem.

2.4. Solution to the Laplace Equation

In order to get the potential distributions in the three subregions, we need to solve the Laplace equation for each region by considering the general solution and boundary conditions. Solution to Laplace equation for subregion 1 is discussed first. Substitution of the first Neumann-type boundary condition in equation (7) into the partial derivative of equation (6) with respect to *x* yields

$$\frac{\partial \phi_1(0,y,t)}{\partial x} = A^1(t)[C^1(t)y + D^1(t)] + \lambda E^1(t) \times [G^1(t)\sinh(\lambda y) + H^1(t)\cosh(\lambda y)] = 0, \forall y, t \text{ and } \lambda \neq 0 \tag{15}$$

where subscript 1 and superscript 1 both denote the subregion 1. This boundary condition can be satisfied by letting $C^1(t) = 0$, $A^1(t)D^1(t) = 0$ and $E^1(t) = 0$. Substitution of the second Neumann-type boundary condition in equation (7) into the partial derivative of equation (6) with respect to *x* leads to

$$\frac{\partial \phi_1(p,y,t)}{\partial x} = -\lambda F^1(t)\sin(\lambda p)[G^1(t)\sinh(\lambda y) + H^1(t)\cosh(\lambda y)] = 0. \quad \forall y, t \text{ and } \lambda \neq 0 \tag{16}$$

This boundary condition can be only met when $\sin(\lambda p) = 0$ for $\lambda \neq 0$ and $F^1(t) \neq 0$ are necessary in this situation, which means that the separation constant

$$\lambda = \frac{n\pi}{p}, \quad n = 1, 2, \ldots, \infty. \tag{17}$$

By introducing the notations $K^1(t) = B^1(t)D^1(t)$, $L^1(t) = F^1(t)G^1(t)$ and $M^1(t) = F^1(t)H^1(t)$, the solution to Laplace equation for subregion 1 can be expressed as

$$\phi_1(x,y,t) = K^1(t) + \sum_{n=1}^{\infty}[L_n^1(t)\sinh(\frac{n\pi y}{p}) + M_n^1(t)\cosh(\frac{n\pi y}{p})]\cos(\frac{n\pi x}{p}). \tag{18}$$

Another boundary condition associated with subregion 1 is the potential distribution on the plane $y = 0$, which has been given by equation (11). Matching the terms in equation (11) with equation (18) at $y = 0$ yields the following two relationships:

$$K^1(t) = \frac{V_p(t)+V_n(t)}{2}, \tag{19}$$

and

$$M_n^1(t) = \frac{2[V_n(t)-V_p(t)]}{n^2\pi^2(1-2w/p)}[\cos(n\pi - \frac{n\pi w}{p}) - \cos(\frac{n\pi w}{p})]. \tag{20}$$

With respect to the solution to Laplace equation for subregion 2, we assume it has a form similar to that of $\phi_1(x,y,t)$, that is,

$$\phi_2(x,y,t) = K^2(t) + \sum_{n=1}^{\infty}[L_n^2(t)\sinh(\frac{n\pi y}{p}) + M_n^2(t)\cosh(\frac{n\pi y}{p})]\cos(\frac{n\pi x}{p}). \tag{21}$$

In subregion 3, a particular boundary condition expressed by equation (14) results in a different form of potential expression as the form in subregion 1, and it can be written as

$$\phi_3(x,y,t) = K^3(t) + \sum_{n=1}^{\infty} L_n^3(t)\exp(\frac{n\pi y}{p})\ \cos(\frac{n\pi x}{p}). \qquad (22)$$

The eight unknown time-varying coefficients in the potential expressions of the three subregions can be obtained by substituting the solutions to Laplace equation for the three subregions into the boundary conditions at the two dielectric interfaces [equations (12) and (13)] and considering the two relationships shown in equations (19) and (20). Here, we take the Laplace transforms of the time functions to circumvent the computational difficulty created by the presence of the time derivatives of field solutions in the boundary conditions [equations (13)]. The Laplace transforms of time domain functions are denoted by replacing the time variable *t* with the complex variable *s*. Hereto, the solutions to Laplace equation for the three subregions can all be solved when we obtain the Laplace transforms of the eight unknown time-varying coefficients $K^1(s)$, $L_n{}^1(s)$, $M_n{}^1(s)$, $K^2(s)$, $L_n{}^2(s)$, $M_n{}^2(s)$, $K^3(s)$, and $L_n{}^3(s)$ (see Appendix).

2.5 Electric field and Electrostatic Adhesion Force

Each of the electric field components in subregions 1, 2, 3 can be derived from equation (1) after we obtain the solutions to Laplace equation for the three regions, which are expressed as the product between the voltage difference $V_\nabla(s)$ and the sum of an infinite series of rational, second-order transfer functions, as follows:

$$E_{r,x}(x,y,s) = \frac{\pi}{p}V_\nabla(s)\sum_{n=1}^{\infty} n\gamma(n)\sin(\frac{n\pi x}{p}) \times \frac{a_{2,x}^r(n,y)s^2 + a_{1,x}^r(n,y)s + a_{0,x}^r(n,y)}{b_2(n)s^2 + b_1(n)s + b_0(n)},$$

$$E_{r,y}(x,y,s) = -\frac{\pi}{p}V_\nabla(s)\sum_{n=1}^{\infty} n\gamma(n)\cos(\frac{n\pi x}{p}) \times \frac{a_{2,y}^r(n,y)s^2 + a_{1,y}^r(n,y)s + a_{0,y}^r(n,y)}{b_2(n)s^2 + b_1(n)s + b_0(n)}. \qquad (23)$$

where $r = 1, 2, 3$ and

$$a_{l,x}^1(n,y) = a_{l,\mathrm{L}_1}(n)\sinh(\frac{n\pi y}{p}) + b_l(n)\cosh(\frac{n\pi y}{p}),$$

$$a_{l,y}^1(n,y) = a_{l,\mathrm{L}_1}(n)\cosh(\frac{n\pi y}{p}) + b_l(n)\sinh(\frac{n\pi y}{p}),$$

$$a_{l,x}^2(n,y) = a_{l,\mathrm{L}_2}(n)\sinh(\frac{n\pi y}{p}) + a_{l,\mathrm{M}_2}(n)\cosh(\frac{n\pi y}{p}),$$

$$a_{l,y}^2(n,y) = a_{l,\mathrm{L}_2}(n)\cosh(\frac{n\pi y}{p}) + a_{l,\mathrm{M}_2}(n)\sinh(\frac{n\pi y}{p}),$$

$$a_{m,x}^3(n,y) = a_{m,y}^3(n,y) = a_{m,\mathrm{L}_3}(n)\exp(\frac{n\pi y}{p}),$$

$$a_{0,x}^3(n,y) = a_{0,y}^3(n,y) = 0,$$

$$l = 0, 1, 2 \qquad m = 1, 2$$

In this work, the electrostatic adhesion force exerted on the dielectric plate can be calculated by using the Maxwell stress tensor formulation. The net *i*th force component on a dielectric medium is obtained by integrating the Maxwell stress tensor $\mathbf{T}_{ij}$ over the enclosing surface S [21],

$$F_i = \varepsilon_0 \oint_s (T_{ij}n_j)dA = \varepsilon_0 \oint_s [(E_iE_j - \frac{1}{2}\delta_{ij}E_kE_k)n_j]dA \qquad (24)$$

where the Einstein convention has been used for vector indices and δ_{ij} is the Kronecker delta. In addition, the integration in equation (24) should take place over the outer boundary of the enclosing surface S. Since $d_4 >> d_2, d_4 >> d_3$ and d_4 is usually treated as infinity for reasonable simplification, the potential on the lower surface of the dielectric plate decays to zero, and the electric field decays to zero as well. This implies that only the electric field solution in subregion 2 is required in the integration, and the electrostatic adhesion force exerted on the dielectric plate of one period can be written as

$$F = \frac{\varepsilon_0 L}{2}\int_0^p [E_{2,y}^2(x,y,t) - E_{2,x}^2(x,y,t)]dx. \qquad (25)$$

The time domain electric filed components required to evaluate the above expression can be obtained straightforwardly by applying the inverse Laplace transform to equation (23).

3. MODEL VERIFICATION AND ANALYSIS

3.1. Field and Force Dynamics Under a Step Voltage Excitation

Since free charges inside a conductor can move freely, these charges will appear on the surface facing the electrodes nearly uniformly immediately after voltages are applied to electrodes. However, in the case of a dielectric, charge collection mainly originates from polarization, which can usually not occur instantaneously. Hence, a dynamic relation, which

includes a time-varying function, exists between the applied electrode voltages and electrostatic adhesion force due to the resistivity of the dielectric or the delayed polarization. In this work, the field and force dynamics are assessed by evaluating the transient response of the field and force under a step in applied voltages, and these are in accord with the actual adhesion process where the voltages exerted to the electrodes may actually behave like a step input. Let us define the step voltages as

$$\begin{cases} V_{\mathrm{p}}(t)=0, & \text{if } t\le 0 \\ V_{\mathrm{p}}(t)=V_{\mathrm{p}}, & \text{if } t>0 \end{cases} \text{ and } \begin{cases} V_{\mathrm{n}}(t)=0, & \text{if } t\le 0 \\ V_{\mathrm{n}}(t)=V_{\mathrm{n}}, & \text{if } t>0 \end{cases}. \tag{26}$$

The Laplace transforms of these step voltages are given by $V_{\mathrm{p}}(s)=V_{\mathrm{p}}/s$ and $V_{\mathrm{n}}(s)=V_{\mathrm{n}}/s$, respectively. Equation (23) demonstrates the relationship between the input voltage $V_{\nabla}(s)$ and each of the field components, which is described by an infinite series of second-order, rational transfer functions, whose denominator and numerator polynomial coefficients are functions of the summation index *n*. Since the transfer function completely represents a system differential equation, its poles, which are the roots of the denominator polynomials, and zeros, which are the roots of the numerator polynomials, can effectively define the system response.

Let $[p_1(n);p_2(n)]$ and $[z_{1,l}^r(n);z_{2,l}^r(n)]$ denote the poles and zeros of the second-order transfer functions in the series expansion of the field components [equation (23)], where the subscript l $(l=x,y)$ refers to the axis orientation of the field component and the superscript r $(r=1,2,3)$ indicates the subregion. The step response of the field in the time domain can be expressed in terms of the poles and zeros on applying the inverse Laplace transform to equation (23), yielding the following field components:

$$E_{r,x}(x,y,t)=\frac{\pi}{p}(V_{\mathrm{p}}-V_{\mathrm{n}})\sum_{n=1}^{\infty}n\gamma(n)\sin(\frac{n\pi x}{p})T_{r,x}(y,n,t)$$

$$E_{r,y}(x,y,t)=\frac{\pi}{p}(V_{\mathrm{p}}-V_{\mathrm{n}})\sum_{n=1}^{\infty}n\gamma(n)\cos(\frac{n\pi x}{p})T_{r,y}(y,n,t) \tag{27}$$

where the time domain function $T_{r,l}(y,n,t)$ is given by

$$\begin{aligned} T_{r,l}(y,n,t)=&\frac{a_{2,l}^r(n,y)}{b_2(n)}\{\frac{z_{1,l}^r(n)z_{2,l}^r(n)}{p_1(n)p_2(n)}+\\ &\frac{[z_{2,l}^r(n)-p_1(n)][z_{1,l}^r(n)-p_1(n)]}{p_1(n)[p_1(n)-p_2(n)]}\times\exp[p_1(n)t]\\ &-\frac{[z_{2,l}^r(n)-p_2(n)][z_{1,l}^r(n)-p_2(n)]}{p_2(n)[p_1(n)-p_2(n)]}\\ &\times\exp[p_2(n)t]\} \end{aligned} \tag{28}$$

where $r=1,2,3$ and $l=x,y$. Hence, the dynamic force expression can be derived by substituting $E_{2,x}(x,y,t)$ and $E_{2,y}(x,y,t)$ into equation (25).

3.2. Evaluation of Adhesion Performance on a Glass Pane

To verify the model developed, adhesion performance of an electrode panel on a glass pane is evaluated. The electrode panel with a pair of interdigital electrodes as shown in Figure **2** is made from a flexible etched printed circuit board by removing copper films. The base of the panel is a polyimide film with $d_2=50\mu\mathrm{m}$. Interdigital electrodes made from the copper film are deposited on the polyimide base, which are then covered by another polyimide film with $d_1=50\mu\mathrm{m}$. The bulk electrical properties of the polyimide films are $\varepsilon_{\mathrm{p}}=3.4\varepsilon_0$ and $\sigma_{\mathrm{p}}=10^{-17}\,\mathrm{S/cm}$, where $\varepsilon_0=8.85\times10^{-12}\,\mathrm{F/m}$ is the permittivity of vacuum. The width of the electrode and the space between neighbouring electrodes are both 1 mm, and the length of the electrode is $L=300\ \mathrm{mm}$. The total area of the electrode panel is $A=300\ \mathrm{mm}\times200\ \mathrm{mm}$. The glass pane has a thickness (d_4) of $5\ \mathrm{mm}$, while the thickness of the air layer between the electrode panel and the glass pane due to the influence of roughness is assumed to be $d_3=20\ \mu\mathrm{m}$. The bulk electrical properties of the glass pane are given by $\varepsilon_{\mathrm{d}}=3.5\varepsilon_0$ and $\sigma_{\mathrm{d}}=10^{-13}\,\mathrm{S/cm}$, and the applied step voltages are $V_{\mathrm{p}}=800\ \mathrm{V}$ and $V_{\mathrm{n}}=-800\ \mathrm{V}$.

Since the series expansion of the field components are summations over an infinite number of terms, they need to be truncated by considering reasonable accuracy of the model and complexity of the computation. A detailed discussion of this problem will be given in the next section. Here, we just show the numerical results carried out by using the numerical software package MATLAB. In addition, experiment work of the electrode panel on the glass pane is conducted, and experimental results and theoretical consequences are both presented to verify the model.

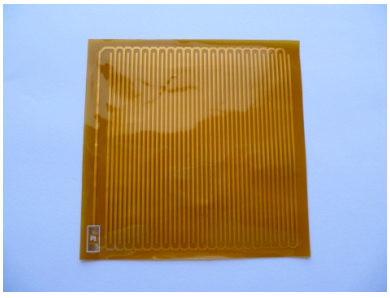

Figure 2: An electrode panel with a pair of interdigital electrodes.

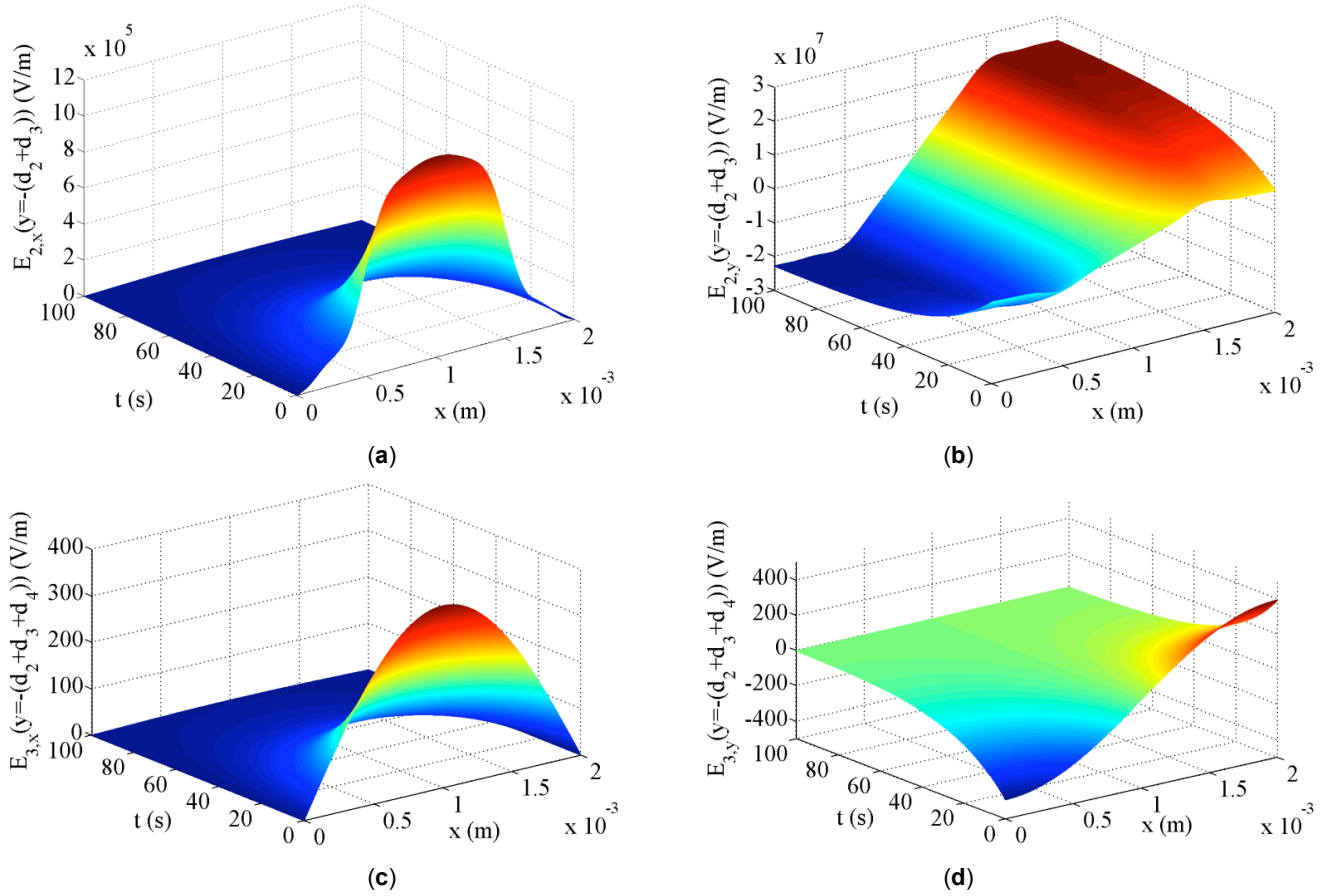

Figure 3: The step response of the electric field components as a function of time (t) and distance (x) along the boundary $y=-(d_2+d_3)$ in region 2 [(**a**) and (**b**)] and $y=-(d_2+d_3+d_4)$ in region 3 [(**c**) and (**d**)].

Figure **3** depicts the time histories of the step response of the field components on the boundary $y=-(d_2+d_3)$ in region 2 [Figure **3**(**a**) and Figure **3**(**b**)] and on the boundary $y=-(d_2+d_3+d_4)$ in region 3 [Figure **3**(**c**) and Figure **3**(**d**)]. These plots show that all field components except for $E_{2,y}(x,y,t)$ decay to zero as the time increases. We also notice that the field components on the boundary $y=-(d_2+d_3+d_4)$ are much smaller than that on the boundary $y=-(d_2+d_3)$, which proves that ignoring the influence of field components on the boundary $y=-(d_2+d_3+d_4)$ in the integration [equation (25)] in calculating the adhesion force is reasonable. Figure **4** depicts the time histories of the electrostatic adhesion force exerted on the glass pane. Both the experimental data and theoretical data demonstrate that it needs almost 100s for the adhesion force to increase gradually to a steady value. The discrepancy between the presented experimental data and the theoretical results mainly results from two aspects: (a) the linear approximation of the potential distribution in the inter electrode gap, which results in the inherent error of the model; (b) the influence of the vacuum suction force, which will be discussed in the following section.

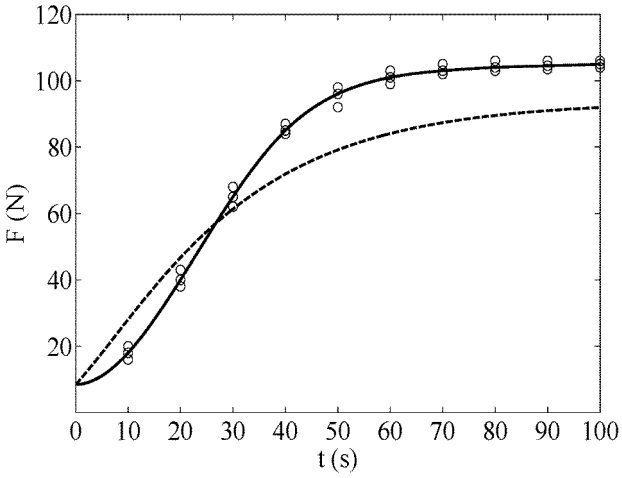

Figure 4: Time histories of the electrostatic adhesion force exerted on the glass pane. Theoretical results (---) and experimental results (—).

4. DISCUSSION

4.1. Approximation of the Interelectrode Potential

The potential distribution on the entire electrode plane, bounded by the plane $y=0$, represents one of the boundary conditions required to determine the field

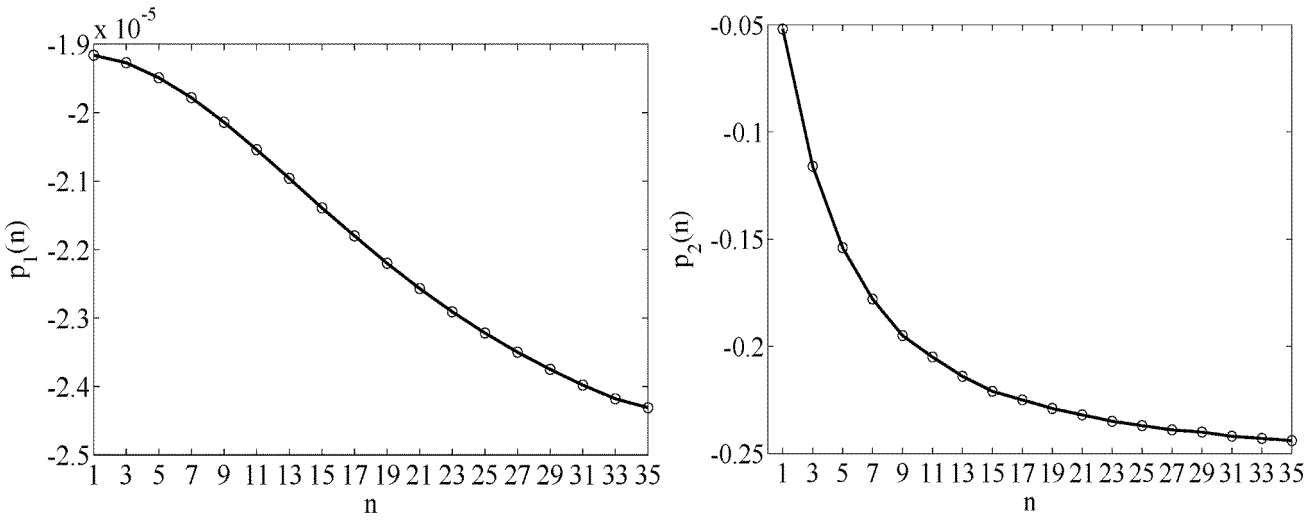

(**a**) (**b**)

Figure 5: Dependency of the transfer function poles $p_1(n)$ [(a)] and $p_2(n)$ [(b)] on summation index n.

distribution in subregion 1. Nevertheless, we apply known voltages only to the electrodes in practical electrode panel while the potential distributions between the electrodes are unknown. In the physical model given above, for clarity and convenience, we take the first-order Taylor series approximation, assuming that the potential varies linearly with distance in the electrode gaps.

Since the electrodes are placed in a homogeneous dielectric medium (the top and bottom surface of the copper electrodes are both covered by a polyimide film), the field in the direction normal to the electrode plane is zero in the electrode gaps. This additional constraint for the electrical field configuration can be used to determine the potentials in the electrode gaps. The approach is as follows. First, the electrical potential in each interelectrode gap is expanded as a Taylor series with respect to the distance from the electrode gap centre with undetermined polynomial coefficients. Then, the expressions for the electrical potential and electric field component everywhere in terms of the undetermined coefficients can be obtained through symbolic calculation. Finally, values for these coefficients are determined by applying the field constraint condition, so that the field results are self-consistent.

The Taylor expansion of the electrical potentials in the electrode gaps is given as follows (even terms disappear due to the electrode symmetry)

$$\phi(x,0,t) = \frac{V_{\mathrm{p}}(t)+V_{\mathrm{n}}(t)}{2} + \frac{[V_{\mathrm{n}}(t)-V_{\mathrm{p}}(t)]}{2} \times \sum_{m=0}^{\infty} \alpha_{2m+1}(x-p/2)^{2m+1} \tag{29}$$

where $w \le x \le p-w$, and the polynomial coefficients α_{2m+1} $(m=0,1,2,...)$ satisfy

$$\sum_{m=0}^{\infty} \alpha_{2m+1}(p/2-w)^{2m+1} = 1 \tag{30}$$

We derive the analytical expressions for the field components and electrostatic adhesion force by substituting $\phi(x,0,t)$ in terms of the undetermined polynomial coefficients α_{2m+1} into the derivation process in section 2, most conveniently by using symbolic manipulation by computer. The polynomial coefficients α_{2m+1} can then be determined from the constraint

$$E_y(x,0,t) = 0 \qquad w \le x \le p-w \tag{31}$$

Practically, a finite number of polynomial terms is taken as an approximation, and an optimization function for determining the coefficients is then used to minimize the error resulting from the finite number of terms

$$\underset{\alpha_1,\alpha_3,...,\alpha_{2m+1}}{\mathrm{Min}} \{\int_w^{p-w} E_y^2(x,0,t)dy\}. \tag{32}$$

Evidently, the optimization procedure results in the smallest magnitude of E_y values in such a way that these magnitudes alternate about zero. Generally, a third or five order approximation for the potential in the

interelectrode gap is adopted by considering the model accuracy and complexity of computation at the same time.

4.2. Truncation of Series Expansions of the Field Components

From a computational point of view, the series expansion of the field components, which involve summations over an infinite number of terms, need to be truncated. The total number (n_{total}) of the summation terms required to sufficiently obtain the field dynamics and achieve reasonable accuracy of the model can be determined by identifying the dominant poles of the second order transfer functions for the field components given by equation (23). Figure **5** depicts the poles $p_1(n)$ and $p_2(n)$ as a function of the summation index *n*. $p_1(n)$ and $p_2(n)$ reflect the different speeds at which charges accumulate on the boundary $y=-d_2$ and on the boundary $y=-(d_2+d_3)$. Since the bulk conductivity of the polyimide film is much smaller than that of the glass panel, charges accumulation is mainly and much quicker at the boundary $y=-(d_2+d_3)$. The dynamic properties of the field and adhesion force are mainly reflected by $p_2(n)$ in the actual application. As the integer *n* varies from 1 to 31, $p_2(n)$ decreases from -0.052 to -0.242. For higher value of *n*, $p_2(n)$ does not decrease apparently but comes to a steady value near -0.25. Meanwhile, we notice that the magnitude of field components decrease sharply as the integer value of *n* increases. Based on the above considerations, the choice of $n_{total}=31$ is verified to lead to a rapid convergence of the sum, and the dynamic properties of field and adhesion force can also be demonstrated well.

4.3. Influence of Vacuum Suction Force

The discrepancy between the theoretical and experimental results of the electrostatic adhesion force is demonstrated in Figure **4**. From the observation of the performance of the electrode panel on the glass pane, it is speculated that vacuum suction force, such as that in a suction cup, is also involved in adhesion. Due to the flexibility of the electrode panel, the small gap with low air pressure is generated, resulting in the vacuum suction force when electrostatic adhesion is activated. At the initial phase of the adhesion, experimental data are smaller than the theoretical data because the contact between the electrode panel and the glass pane is not close enough, which certainly reduces the adhesion force. As the adhesion force gradually increases with time, the electrode panel contact more closely with the glass pane. Meanwhile, the air beneath the electrode panel is squeezed out and the negative pressure environment is formed, resulting in the vacuum suction force exerted on the electrode panel. The theoretical data are larger than the experimental data when the adhesion reaches a steady value at the final phase because of the influence of the vacuum suction force.

5. CONCLUSIONS

This paper has introduced an analytical model to analyze the dynamic properties of the electric field and electrostatic adhesion force generated by interdigital electrode arrays. The expressions of electric filed components are derived by solving the Laplace equation for the electrical potential in each subregion. The electrostatic adhesion force is calculated by using the Maxwell stress tensor formulation. Experiments are carried out to verify the model by evaluating the adhesion performance of an electrode panel on a glass pane. We find a relatively good agreement between theory and experiment. An approximation method for the potential distribution in the interelectrode gap is discussed in detail, which can further improve the model accuracy. In addition, we find that vacuum suction force is involved in the adhesion. The influence of this vacuum suction force to electrostatic adhesion is also discussed.

The model proposed in this paper is not specific for a single problem but universal to many electrostatic adhesion problems, where interdigital electrodes are utilized to generate electric field and electrostatic adhesion force, such as the electrostatic chuck and electrostatic suspension system used in industry areas, and wall-climbing robots using electrostatic adhesion force. The outcome of this work can provide support for theoretical guidelines and system optimization for these electrostatic applications. Further study is needed to analyze the important factors which influence the electrostatic adhesion problem, especially the dynamic response speed of the adhesion force. Another area for future investigation can be focused on the mathematical modelling of the surface roughness instead of the simplified uniform air layer in this paper.

ACKNOWLEDGEMENTS

This research is supported by The National Key Technology R&D Program (Grant no. 2012BAF12B09) and The Key Science and Technology Project of Chongqing (Grant no. cstc2013gg-yyjsB70001).

APPENDIX: SOLUTION TO THE LAPLACE EQUATION

The Laplace equation was solved by symbolic computations of the software package called MATLAB. The analytical solutions of the Laplace transforms of the eight unknown time-varying coefficients were given by:

$$K^1(s) = K^2(s) = K^3(s) = \frac{1}{2}[V_{\mathrm{p}}(s) + V_{\mathrm{n}}(s)],$$

$$L_n^1(s) = V_{\nabla}(s)\gamma(n)\frac{a_{2,\mathrm{L}_1}(n)s^2 + a_{1,\mathrm{L}_1}(n)s + a_{0,\mathrm{L}_1}(n)}{b_2(n)s^2 + b_1(n)s + b_0(n)},$$

$$L_n^2(s) = V_{\nabla}(s)\gamma(n)\frac{a_{2,\mathrm{L}_2}(n)s^2 + a_{1,\mathrm{L}_2}(n)s + a_{0,\mathrm{L}_2}(n)}{b_2(n)s^2 + b_1(n)s + b_0(n)},$$

$$L_n^3(s) = V_{\nabla}(s)\gamma(n)\frac{a_{2,\mathrm{L}_3}(n)s^2 + a_{1,\mathrm{L}_3}(n)s}{b_2(n)s^2 + b_1(n)s + b_0(n)},$$

$$M_n^1(s) = V_{\nabla}(s)\gamma(n),$$

$$M_n^2(s) = V_{\nabla}(s)\gamma(n)\frac{a_{2,\mathrm{M}_2}(n)s^2 + a_{1,\mathrm{M}_2}(n)s + a_{0,\mathrm{M}_2}(n)}{b_2(n)s^2 + b_1(n)s + b_0(n)},$$

where

$$V_{\nabla}(s) = V_p(s) - V_n(s),$$

$$\gamma(n) = \begin{cases} 0 & n = \text{even} \\ \dfrac{4\cos(n\pi w / p)}{n^2\pi^2(1 - 2w/p)} & n = \text{odd} \end{cases},$$

and the numerator polynomial coefficients, which are functions of the summation index n, are defined as

$$a_{2,\mathrm{L}_1}(n) = {\varepsilon_0}^2\cosh(\frac{n\pi d_2}{p})\sinh(\frac{n\pi d_3}{p}) + \varepsilon_0\varepsilon_{\mathrm{p}}\cosh(\frac{n\pi d_3}{p}) \times \sinh(\frac{n\pi d_2}{p}) + \varepsilon_{\mathrm{d}}\varepsilon_{\mathrm{p}}\sinh(\frac{n\pi d_3}{p})\sinh(\frac{n\pi d_2}{p}) + \varepsilon_0\varepsilon_{\mathrm{d}}\cosh(\frac{n\pi d_3}{p})\cosh(\frac{n\pi d_2}{p}),$$

$$a_{1,\mathrm{L}_1}(n) = \varepsilon_0\sigma_{\mathrm{d}}\cosh(\frac{n\pi d_2}{p})\cosh(\frac{n\pi d_3}{p}) + \varepsilon_0\sigma_{\mathrm{p}}\cosh(\frac{n\pi d_3}{p}) \times \sinh(\frac{n\pi d_2}{p}) + \varepsilon_{\mathrm{d}}\sigma_{\mathrm{p}}\sinh(\frac{n\pi d_3}{p})\sinh(\frac{n\pi d_2}{p}) + \varepsilon_{\mathrm{p}}\sigma_{\mathrm{d}}\sinh(\frac{n\pi d_3}{p})\sinh(\frac{n\pi d_2}{p}),$$

$$a_{0,\mathrm{L}_1}(n) = \sigma_{\mathrm{d}}\sigma_{\mathrm{p}}\sinh(\frac{n\pi d_2}{p})\sinh(\frac{n\pi d_3}{p}),$$

$$a_{2,\mathrm{L}_2}(n) = \varepsilon_{\mathrm{p}}\varepsilon_{\mathrm{d}}\cosh[\frac{n\pi(d_2 + d_2)}{p}] + \varepsilon_0\varepsilon_{\mathrm{p}}\sinh[\frac{n\pi(d_2 + d_2)}{p}],$$

$$a_{1,\mathrm{L}_2}(n) = \sigma_{\mathrm{p}}\varepsilon_{\mathrm{d}}\cosh[\frac{n\pi(d_2 + d_3)}{p}] + \varepsilon_0\sigma_{\mathrm{p}}\sinh[\frac{n\pi(d_2 + d_3)}{p}] + \varepsilon_{\mathrm{p}}\sigma_{\mathrm{d}}\cosh[\frac{n\pi(d_2 + d_3)}{p}],$$

$$a_{0,\mathrm{L}_2}(n) = \sigma_{\mathrm{d}}\sigma_{\mathrm{p}}\cosh[\frac{n\pi(d_2 + d_3)}{p}],$$

$$a_{2,\mathrm{L}_3}(n) = \varepsilon_0\varepsilon_{\mathrm{p}}\exp[\frac{n\pi(d_2 + d_3)}{p}],$$

$$a_{1,L_3}(n) = \varepsilon_0\sigma_p \exp[\frac{n\pi(d_2+d_2)}{p}],$$

$$a_{2,M_2}(n) = \varepsilon_p\varepsilon_d \sinh[\frac{n\pi(d_2+d_3)}{p}] + \varepsilon_0\varepsilon_p \cosh[\frac{n\pi(d_2+d_3)}{p}],$$

$$a_{1,L_2}(n) = \sigma_p\varepsilon_d \sinh[\frac{n\pi(d_2+d_3)}{p}] + \varepsilon_0\sigma_p \cosh[\frac{n\pi(d_2+d_3)}{p}] + \varepsilon_p\sigma_d \sinh[\frac{n\pi(d_2+d_3)}{p}],$$

$$a_{0,L_2}(n) = \sigma_d\sigma_p \sinh[\frac{n\pi(d_2+d_3)}{p}],$$

and finally the denominator polynomial coefficients are given by

$$b_2(n) = \varepsilon_0{}^2 \sinh(\frac{n\pi d_2}{p})\sinh(\frac{n\pi d_3}{p}) + \varepsilon_0\varepsilon_p \cosh(\frac{n\pi d_3}{p}) \times \cosh(\frac{n\pi d_2}{p}) + \varepsilon_d\varepsilon_p \sinh(\frac{n\pi d_3}{p})\cosh(\frac{n\pi d_2}{p}) + \varepsilon_0\varepsilon_d \cosh(\frac{n\pi d_3}{p})\sinh(\frac{n\pi d_2}{p}),$$

$$b_1(n) = \varepsilon_0\sigma_d \sinh(\frac{n\pi d_2}{p})\cosh(\frac{n\pi d_3}{p}) + \varepsilon_0\sigma_p \cosh(\frac{n\pi d_3}{p}) \times \cosh(\frac{n\pi d_2}{p}) + \varepsilon_d\sigma_p \sinh(\frac{n\pi d_3}{p})\cosh(\frac{n\pi d_2}{p}) + \varepsilon_p\sigma_d \sinh(\frac{n\pi d_3}{p})\cosh(\frac{n\pi d_2}{p}),$$

$$b_0(n) = \sigma_d\sigma_p \cosh(\frac{n\pi d_2}{p})\sinh(\frac{n\pi d_3}{p}).$$

REFERENCES

[1] Castle GSP. The evolving field of electrostatics. Institute of Physics Conference Series 1991; 118: 1-12.

[2] Yatsuzuka K, Hatakeyama F, Asano K, Aonuma S. Fundamental characteristics of electrostatic wafer chuck with insulating sealant. IEEE Trans. Ind. Appl. 2000; 36(2): 510-516. http://dx.doi.org/10.1109/28.833768

[3] Asano K, Hatakeyama F, Yatsuzuka K. Fundamental study of an electrostatic chuck for silicon wafer handling. IEEE Trans Ind Appl 2002; 38: 840-845. http://dx.doi.org/10.1109/TIA.2002.1003438

[4] Jeop JU, Higuchi T. Electrostatic suspension of dielectrics. IEEE Trans Ind Electron 1998; 45: 938-946. http://dx.doi.org/10.1109/41.735338

[5] Ju J, Yih TC, Higuchi T, Jeon JU. Direct electrostatic levitation and propulsion of silicon wafer handling. IEEE Trans Ind Appl 1998; 34: 975-984. http://dx.doi.org/10.1109/28.720437

[6] Jeon JU, Park K, and Higuchi T. Contactless suspension and transportation of glass panels by electrostatic forces. Sens Actuator A-Phys 2007; 134: 565-574. http://dx.doi.org/10.1016/j.sna.2006.05.016

[7] Green NG, Ramos A, Morgan H. Numerical solution of the dielectrophoretic and travelling wave forces for interdigitated electrode arrays using the finite element method. J Electrost 2002; 56: 235-254. http://dx.doi.org/10.1016/S0304-3886(02)00069-4

[8] Wang XJ, Wang XB, Becker FF, Gascoyne PRC. A theoretical method of electrical field analysis for dielectrophoretic electrode arrays using Green's theorem. J Phys D: Appl Phys 1996; 29: 1649-1660. http://dx.doi.org/10.1088/0022-3727/29/6/035

[9] Garcia M, Clague D. The 2D electric field above a planar sequence of independent strip electrodes. J Phys D: Appl Phys 2000; 33: 1747-1755. http://dx.doi.org/10.1088/0022-3727/33/14/315

[10] Morgan H, Izquierdo AG, Bakewell D, Green NG, Romos A. The dielectrophoretic and travelling wave forces generated by interdigitated electrode arrays: analytical solution using Fourier series. J Phys D: Appl Phys 2001; 34: 1553-1561. http://dx.doi.org/10.1088/0022-3727/34/10/316

[11] Yamamoto A, Nakashima T, Higuchi T. Wall climbing mechanisms using electrostatic attraction generated by flexible electrodes, Int. Symp. on Micro-Nano Mechatronics and Human Science 2007; 389-394.

[12] Prahlad H, Pelrine R, Stanford S, Marlow J, Kornbluh R. Electroadhesive robots—Wall climbing robots enabled by a novel, robust, and electrically controllable adhesion technology. IEEE Int Conf on Robotics and Automation 2008; 3028-3033.

[13] Liu R, Chen R, Shen H, Zhang R. Wall climbing robot using electrostatic adhesion force generated by flexible interdigital electrodes. Int J Adv Robot Syst 2013; 10: 1-9.

[14] Schnelle T, Hagedorn R, Fuhr G, Fiedler S, Muller T. Three-dimensional electric field traps for manipulation of cells—calculation and experimental verification. Biochim Biophys Acta 1993; 1157: 127-140. http://dx.doi.org/10.1016/0304-4165(93)90056-E

[15] Wang XB, Huang Y, Burt J P H, Markx GH, Pethig R. Selective dielectrophoretic confinement of bioparticles in potential energy wells. J Phys D: Appl Phys 1993; 26: 1278-1285. http://dx.doi.org/10.1088/0022-3727/26/8/019

[16] Hughes MP, Pethig R, Wang XB. Dielectrophoretic force on particles in travelling electric fields. J Phys D: Appl Phys 1996; 29: 474-482. http://dx.doi.org/10.1088/0022-3727/29/2/029

[17] Marcuse D. Electrostatic field of coplanar lines computed with the point matching method. IEEE J Quantum Electron 1989; 25: 939-947. http://dx.doi.org/10.1109/3.27984

[18] Woo SJ, Higuchi T. Electric field and force modeling for electrostatic levitation of lossy dielectric plates. J Appl Phys 2010; 108:104906. http://dx.doi.org/10.1063/1.3487938

[19] Haus HA, Melcher JR. Electromagnetic Fields and Energy. NJ: Prentice Hall 1989.

[20] Zhang ZW. Modeling and analysis of electrostatic force for robot handling of fabric materials. IEEE-ASME Trans Mechatron 1999; 4: 39-49.
http://dx.doi.org/10.1109/3516.752083

[21] Melcher R. Continuum Electromechanics. Camb-ridge MA: MIT Press 1981.

Received on 26-12-2014 Accepted on 09-01-2015 Published on 15-01-2015

DOI: http://dx.doi.org/10.15377/2409-9694.2014.01.02.5

© 2014 Chen *et al.*; Avanti Publishers.
This is an open access article licensed under the terms of the Creative Commons Attribution Non-Commercial License (http://creativecommons.org/licenses/by-nc/3.0/) which permits unrestricted, non-commercial use, distribution and reproduction in any medium, provided the work is properly cited.